JACS
JOURNAL OF THE AMERICAN CHEMICAL SOCIETY
Article
pubs.acs.org/JACS

Highly Anisotropic Rhenium(IV) Complexes: New Examples of Mononuclear Single-Molecule Magnets

José Martínez-Lillo,[†,*] Teresa F. Mastropietro,[§] Elsa Lhotel,[∥] Carley Paulsen,[∥] Joan Cano,[†,‡] Giovanni De Munno,[§] Juan Faus,[†,*] Francesc Lloret,[†] Miguel Julve,[†] Saritha Nellutla,[⊥,¶] and J. Krzystek*[,⊥]

[†]Departament de Química Inorgànica/Instituto de Ciencia Molecular (ICMol), Universitat de València, C/Catedrático José Beltrán 2, 46980 Paterna (València), Spain

[‡]Fundació General de la Universitat de València (FGUV), Universitat de València, 46010 València, Spain

[§]Centro di Eccellenza CEMIF.CAL, Dipartimento di Chimica, Università della Calabria, 87030 Arcavacata di Rende, Cosenza, Italy

[∥]Institut Néel-CNRS, BP 166, 25 Avenue des Martyrs, 38042 Grenoble Cedex 9, France

[⊥]National High Magnetic Field Laboratory, Florida State University, Tallahassee, Florida 32310, United States

Supporting Information

ABSTRACT: The rhenium(IV) complex $(NBu_4)_2[ReBr_4(ox)]$ (**1**) (ox = oxalate and NBu_4^+ = tetra-*n*-butylammonium cation) has been prepared and its crystal structure determined by X-ray diffraction. The structure is made up of discrete $[ReBr_4(ox)]^{2-}$ anions and bulky NBu_4^+ cations. Each $[ReBr_4(ox)]^{2-}$ anion is surrounded by six NBu_4^+ cations, which preclude any significant intermolecular contact between the anionic entities, the shortest rhenium···rhenium distance being 9.373(1) Å. Variable temperature dc and ac magnetic susceptibility measurements and field-dependent magnetization experiments on polycrystalline samples of **1** reveal the occurrence of highly anisotropic magnetically isolated Re(IV) centers (S_{Re} = 3/2), which exhibit slow relaxation of the magnetization at very low temperatures in a dc field. Ac measurements conducted on a polycrystalline sample of the complex $(NBu_4)_2[ReCl_4(ox)]$ (**2**) [compound isostructural to **1** whose structure and dc magnetic susceptibility study were previously reported in Tomkiewicz, A.; Bartczak, T. J.; Kruszyński, R.; Mroziński, J. *J. Mol. Struct.* **2001**, *595*, 225] show a similar behavior, both complexes thus constituting new examples of mononuclear single-molecule magnets. High-frequency and -field electron paramagnetic resonance on polycrystalline samples of **1** and **2** and on single crystals of **2** allowed for the determination for the first time of the negative sign and confirmed a significant magnitude and rhombicity (E/D) of the zero-field splitting tensor of the $[ReCl_4(ox)]^{2-}$ and $[ReBr_4(ox)]^{2-}$ centers, originating from a combination of spin−orbit coupling and low molecular symmetry. D and E values of **1** and **2** were estimated through magnetization measurements and theoretically calculated through complete active space and density functional theory methodologies.

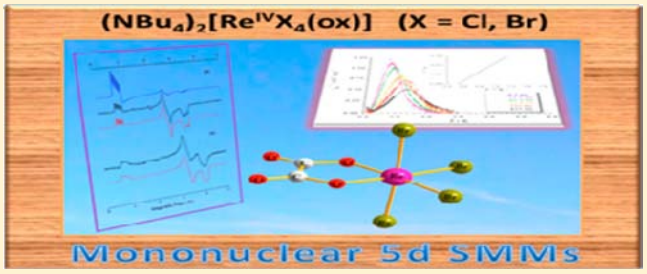

1. INTRODUCTION

Nanoscale molecule-based magnetic materials have attracted extensive and multidisciplinary attention in the last several years due to the unique finite size and quantum mechanical properties that they possess.[1] Single-molecule magnets (SMMs) are among this class of materials, and they represent the smallest possible magnetic device and, hence, a molecular bottom-up approach to nanoscale magnetism.[1,2] The energy barrier to magnetization relaxation in these systems is derived from the anisotropy of the low-lying spin state rather than the movement of domain walls, as in bulk magnets. The main requirements to observe such a behavior in molecules are a high-spin ground state (S) and a significant negative axial zero-field splitting (zfs) parameter D of such a ground state. The upper limit of the energy barrier ($E^{\#}$) for the reorientation of the magnetization vector is given by $S^2|D|$ or $(S^2 - 1/4)|D|$ for integer and half-integer S values, respectively. Potential applications for these materials lie in the fields of high density information storage, quantum computing,[2] and molecular spintronics, among others.[3] The most intensely studied SMMs are those belonging to the family of dodecanuclear complexes of general formula $[Mn_{12}O_{12}(O_2CR)_{16}(H_2O)_4]$ and also, more recently, the series of hexanuclear oxime-based $[Mn_6]$ compounds, where the source of magnetic anisotropy is due to the presence of Mn(III) ions that exhibit an axial Jahn−Teller distortion. Such systems display large values for the energy barrier to the magnetization relaxation.[4]

The need for a better understanding of the quantum tunneling of the magnetization and the mechanisms for slow magnetic relaxation has led this research activity toward mononuclear single-molecule magnets. Recently, SMMs

Received: April 15, 2013
Published: August 19, 2013

   dx.doi.org/10.1021/ja403154z | *J. Am. Chem. Soc.* 2013, 135, 13737−13748

containing only a single lanthanide (4f) ion as the magnetic center housed within porphyrins/phthalocyanins,[5] or polyoxometallates,[6a−c] or ligated in a different way[6d−f] have been reported. As a natural extension of these studies, very recent reports on actinide complexes based on U(III) (5f ion),[7] a linear Fe(I) complex,[8a] a trigonal pyramidal Fe(II) compound,[8b−e] a five-coordinate Fe(III) complex,[8f] and tetrahedral,[9a,b] square-pyramidal,[9c] and six-coordinate Co(II) (all 3d ions) species[9d,e] have revealed them to be mononuclear SMMs. However, as far as we know, no examples of mononuclear SMMs involving 4d or 5d metal ions have yet been explored.

Having these results in mind and in order to fill the existing gap between the 3d and 5f mononuclear SMMs, we focus here on the Re(IV) center (a 5d metal ion). This cation is particularly appealing because in a six-coordinate environment, it has three unpaired electrons (S = 3/2), an orbitally nondegenerate $^4A_{2g}$ ground electronic term, and a large magnetic anisotropy arising from spin−orbit coupling associated with the 5d metal ions. Re(IV) complexes such as $[ReX_4(ox)]^{2-}$ (X = Cl and Br)[10,11] or $[ReCl_4(CN)_2]^{2-}$ [12] when combined with first-row transition metal ions have previously afforded new examples of mixed 5d-3d polynuclear SMMs[10c,f,i] and single-chain magnets,[12] respectively. In this work, we report a magneto-structural study of the isostructural $[ReX_4(ox)]^{2-}$ [X = Br(**1**) and Cl(**2**)] species, which constitute the first examples of 5d-based mononuclear SMMs.

2. EXPERIMENTAL SECTION

2.1. Materials. All starting chemicals and solvents were purchased from commercial sources and used without further purification. Compound $(NBu_4)_2[ReCl_4(ox)]$ (**2**) (NBu_4^+ = tetra-*n*-butylammonium cation) was synthesized by following a previously reported procedure.[11a,13] The complex $(NBu_4)_2[ReBr_4(ox)]$ (**1**) was prepared as described for the parent $(PPh_4)_2[ReBr_4(ox)]$ (PPh_4^+ = tetraphenylphosphonium cation) compound using NBu_4Cl instead of PPh_4Cl as the precipitating agent.[11a] The yield after collecting the different crops was ca. 75%. X-ray-quality crystals of **1** were obtained from the mother liquor as pale green parallelepipeds through slow solvent evaporation at room temperature. A 4:1 Br/Re molar ratio was found for **1** by means of a Philips XL-30 scanning electron microscope (SEM) equipped with a system of X-ray microanalysis from the Central Service for the Support to Experimental Research (SCSIE) at the University of València, and its formula was established by X-ray diffraction on single crystals.

2.2. Physical Measurements. Magnetic susceptibility measurements of a polycrystalline sample of **1** were carried out on a Quantum Design SQUID magnetometer in the temperature range of 2.0−300 K and in an applied magnetic field of 1 T ($T \geq 100$ K) and 250 G ($T <$ 100 K) in order to avoid magnetic saturation. Magnetization measurements of **1** both of a solid sample and in acetonitrile solution were performed in the temperature range 2.0−10 K in applied direct current (dc) fields, covering the range of 0−7 T. Low-temperature alternating current (ac) magnetic susceptibility measurements for **1** and **2** were performed with a SQUID magnetometer equipped with a miniature dilution refrigerator developed at the Institut Néel-CNRS in Grenoble. Vacuum grease was mixed with **1** and **2** and pressed in a small Cu pouch in order to ensure a good thermal contact at low temperature. Oscillating fields of 3 (for $T > 2.0$ K) and 4 G (for $T <$ 2.0 K) in an operating frequency range of 1−1000 Hz and in dc applied fields covering the range of 1500−5000 G were used for the ac measurements on **1** and **2**. All magnetic data were corrected for the diamagnetic contributions of the constituent atoms and also for the sample holder (solid samples) as well as for the solvent (solution sample). High-frequency and -field electron paramagnetic resonance (HFEPR) spectra were recorded at 240 GHz and low temperatures ($T <$ 30 K) on an oriented single crystal of **2** in a super heterodyne spectrometer associated with a 12.5 T superconducting magnet, as previously described.[14] Further experiments were performed on polycrystalline samples of **1** (ca. 50 mg) and **2** (ca. 30 mg) and at multiple frequencies in a 50−640 GHz range in a homodyne spectrometer associated with a 15/17 T superconducting magnet reported before.[15] Detection was provided with a Schottky mixer in the former case and an InSb hot electron bolometer (QMC Ltd., Cardiff, U.K.) in the latter one. The magnetic field was modulated at 20−50 kHz for detection purposes. A Stanford Research Systems SR830 lock-in amplifier converted the modulated signal to dc voltage. The HFEPR spectra were simulated by either software SPIN (A. Ozarowski, NHMFL) or XSophe (Bruker Biospin).

2.3. Computational Details. All calculations of the zfs parameters were performed with the version 2.8 of the ORCA program system.[16] A *TZVP* basis set proposed by Ahlrichs and tight SCF criteria were used in all cases.[17,18] For density functional (DF) calculations, resolution of the identity (RI) approximation with the auxiliary *TZV/J* Coulomb fitting basis sets were employed.[19] For complete active space (CAS) calculations, this auxiliary basis set was replaced by *TZV/C*.[20−22] The *BLYP* and *PBE* functionals were used for DFT calculations.[23−26] Experimental geometries of both $[ReX_4(ox)]^{2-}$ complexes (Tables S2 and S3 of the Supporting Information) were used in the theoretical study. All calculations were done in gas phase and in solution, including electronic effects of the solvent (acetonitrile) by "conductor-like screening model" (COSMO).[27] DF calculations of the zfs were carried out using the quasi-restricted theory.[28] The spin−orbit and spin−spin coupling operators were based on the SOMF scheme.[28] The zfs parameters were evaluated from CAS calculations by including contributions from quartet and doublet states generated from electron promotion between d orbitals. In such cases, in order to verify the influence of the active space on the values of zfs parameters, 10 quartet and 10 doublet states were used in a first approach and then 10 and 20 states, respectively, which corresponds to the full active space built from only the five d orbitals of the rhenium(IV) ion. Because rhenium is a heavy element, relativistic effects can be important. Thus, such effects on the electronic energy were introduced from zero-order regular approximation (ZORA) and Douglas-Kroll-Hess (DKH) formalisms.[29−31] A short molecular dynamics (1531.9 fs) at 10 K from an optimized geometry of **2** was used, using the PBE functional and Born−Oppenheimer molecular dynamics model such as was implemented in Gaussian09.[32,33] In this case, double-ζ and Los Alamos effective core potentials proposed by Hay and Wadt were used.[34−36] Trajectories and initial conditions were carried out from previously calculated vibrational modes and VENUS,[37] respectively. Electronic effects by surrounding molecules in the network were simulated with a polarizable continuum model with the parameters corresponding to the acetonitrile solvent.[38]

2.4. X-ray Data Collection and Structure Refinement. A crystal of **1** with dimensions 0.08 × 0.06 × 0.04 mm^3 was used for diffraction data collection on a Bruker-Nonius X8 APEX II CCD area detector diffractometer, using monochromated Mo Kα radiation (λ = 0.71073 Å). A total of 3908 frames of data were collected using a narrow-frame method with scan widths of 0.3° in φ and ω with exposure time of 10 s per frame using a crystal-to-detector distance of 50 mm. The unit cell parameters were based upon least-squares refinement of 9255 reflections. Data collection was carried out in the range $1.76° > \theta > 26.38°$, and the processing was done through SAINT[39] reduction and SADABS[40] absorption. Of the 86987 collected reflections, 7620 of them were unique [$I < 2\sigma(I)$] and were used for refinement of the structure. The structure of **1** was solved by direct methods and subsequently completed by Fourier recycling using SHELXTL.[41] All nonhydrogen atoms of **1** were refined anisotropically, whereas all hydrogen atoms were set in calculated positions and refined as riding atoms. Full-matrix least-squares refinements on F^2 were carried out by minimizing the function $\sum_w(|F_o| - |F_c|)^2$, and they reached convergence with values of the discrepancy indices given in Table 1. The final geometrical calculations were carried out with PARST97,[42] whereas the graphical manipulations were performed with the XP utility of the SHELXTL system. Selected bond lengths and angles for **1** are listed in Table 2.

Table 1. Crystal Data and Structure Refinement for Compound 1

empirical formula	$C_{34}H_{72}Br_4N_2O_4Re$	
formula weight	1078.78	
temperature	273(2) K	
wavelength	0.71073 Å	
crystal system	monoclinic	
space group	$P2_1/n$	
unit cell dimensions	a = 17.0002(11) Å	α = 90°
	b = 15.8643(9) Å	β = 111.372(2)°
	c = 18.0671(11) Å	γ = 90°
volume	4537.6(5) Å^3	
Z	4	
density (calculated)	1.579 Mg/m^3	
absorption coefficient	6.233 mm^{-1}	
F(000)	2148	
crystal size	0.08 × 0.06 × 0.04 mm^3	
θ range for data collection	1.76 to 26.38°	
index ranges	$-21 \le h \le 21$, $-19 \le k \le 19$, $-22 \le l \le 22$	
reflections collected	86987	
independent reflections	9255 [R(int) = 0.0338]	
completeness to theta = 26.38°	99.7%	
refinement method	full-matrix least-squares on F^2	
data/restraints/parameters	9255/0/406	
goodness-of-fit on F^2	1.006	
final R indices [$I > 2\sigma(I)$]	$R1$ = 0.0234, $wR2$ = 0.0507	
R indices (all data)	$R1$ = 0.0340, $wR2$ = 0.0547	
Largest difference peak and hole	0.746 and −0.685 e Å^{-3}	

3. RESULTS AND DISCUSSION

3.1. Description of the Crystal Structure of $(NBu_4)_2[ReBr_4(ox)]$ (1). The structure of **1** consists of discrete $[ReBr_4(ox)]^{2-}$ anionic units and NBu_4^+ cations. A perspective drawing of the anionic complex in **1** together with the atom numbering is depicted in Figure 1. Compound **1** is isostructural with the analogous chloro compound of formula $(NBu_4)_2[ReCl_4(ox)]$ (**2**).[13]

Each Re(IV) ion in **1** is six-coordinate with two oxygen atoms from a bidentate oxalate and four peripheral bromo atoms building a somewhat distorted octahedral surrounding. One of the main sources of the distortion of the rhenium environment is the reduced bite angle of the oxalate ligand [O(1)−Re−O(2) = 79.73(9)°]. No significant differences were found in the Re−Br and Re−O bond lengths (average values of 2.491(1) and 2.021(2) Å, respectively). The Re−Br bond lengths in the trans position to the oxygen donors [main value 2.4791(4) Å] are just slightly shorter than those in the cis one [average value 2.503(1) Å]. These values are all in agreement with those found in the literature for other similar compounds.[10,11] The O(1)O(2)Br(1)Br(2) set of atoms defines the best equatorial plane around the Re(1) atom, the largest deviation from planarity being 0.010(1) Å for the O(1) and O(2) atoms. The Re(1) atom is shifted by only 0.004(1) Å from this plane. The oxalate ligand is planar and forms a dihedral angle of 1.6(1)° with the mean equatorial plane. The complex anions are well-separated from each other in the resulting three-dimensional ionic lattice, due to the presence of the bulky tetra-*n*-butylammonium cations which are interposed between them (Figure 2). Each $[ReBr_4(ox)]^{2-}$ entity is surrounded by six closest neighboring cations [the Re···N distances varying in the range 5.674(3)−7.757(2) Å] (Figure 2, left) which interact with the anionic complex by means of electrostatic forces and multiple Br···H−C [values ranging from 2.849(1) to 3.259(1) Å] and O···H−C type [values in the range of 2.457(2)−3.199(2) Å] weak supramolecular interactions (Figure 2, right). The shortest Re···Re separation is 9.373(1) Å [Re(1)···Re(1a); symmetry code: $a = 1 - x, 1 - y, -z$], a value which is very close to that observed in the parent chloro derivative [ca. 9.293(1) Å (**2**)].[13] These large interionic metal−metal distances in **1** and **2** preclude the occurrence of any short contact between the ligand atoms of adjacent anions.

Table 2. Bond Lengths (Å) and Angles (°) for 1

Re(1)−O(2)	2.021(2)
Re(1)−O(1)	2.022(2)
Re(1)−Br(2)	2.4745(4)
Re(1)−Br(1)	2.4836(4)
Re(1)−Br(3)	2.4981(4)
Re(1)−Br(4)	2.5074(4)
C(24)−C(25)	1.502(4)
C(25)−C(26)	1.505(5)
C(27)−C(28)	1.508(4)
C(28)−C(29)	1.514(5)
C(29)−C(30)	1.517(5)
C(31)−C(32)	1.505(4)
C(32)−C(33)	1.514(5)
C(33)−C(34)	1.497(5)
O(2)−Re(1)−O(1)	79.73(9)
O(2)−Re(1)−Br(2)	92.98(6)
O(1)−Re(1)−Br(2)	172.68(6)
O(2)−Re(1)−Br(1)	173.06(6)
O(1)−Re(1)−Br(1)	93.33(6)
Br(2)−Re(1)−Br(1)	93.955(13)
O(2)−Re(1)−Br(3)	89.19(7)
O(1)−Re(1)−Br(3)	87.69(7)
Br(2)−Re(1)−Br(3)	91.549(16)
Br(1)−Re(1)−Br(3)	90.836(13)
O(2)−Re(1)−Br(4)	88.24(7)
O(1)−Re(1)−Br(4)	89.70(7)
Br(2)−Re(1)−Br(4)	90.770(16)
Br(1)−Re(1)−Br(4)	91.448(15)
Br(3)−Re(1)−Br(4)	176.627(15)

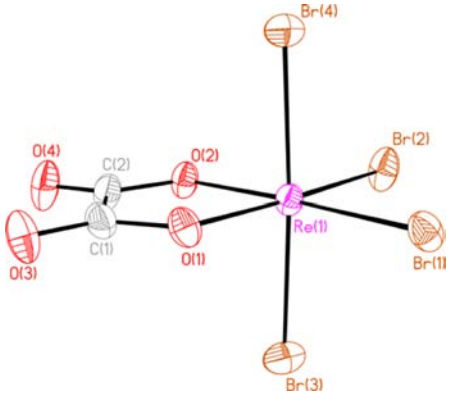

Figure 1. Perspective drawing of the $[ReBr_4(ox)]^{2-}$ unit of **1**, showing the atom numbering. Thermal ellipsoids are drawn at the 30% probability level.

dx.doi.org/10.1021/ja403154z | J. Am. Chem. Soc. 2013, 135, 13737−13748

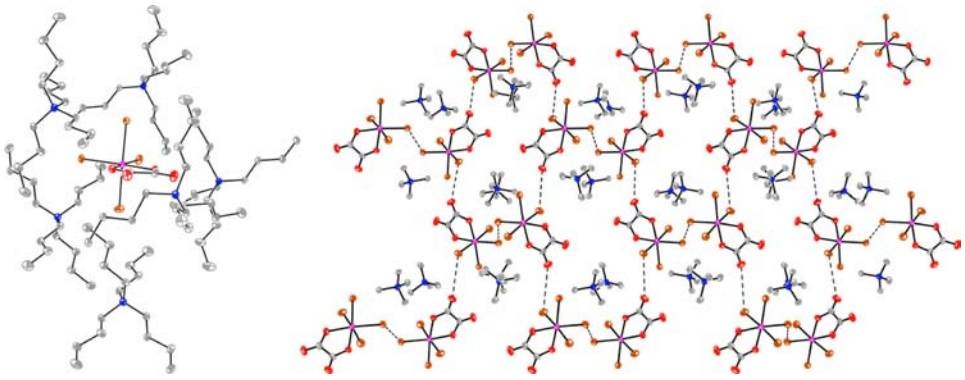

Figure 2. (Left) View of a fragment of the crystal packing of **1** showing the relative arrangement of a $[Re^{IV}Br_4(ox)]^{2-}$ anion and the nearest tetra-*n*-butylammonium cations. (Right) Perspective view of the relative disposition of nearest $[Re^{IV}Br_4(ox)]^{2-}$ anions in **1** showing the shortest Br···Br and Br···O distances as dashed lines (only the NC_4 skeleton of the tetra-*n*-butylammonium cations is drawn for the sake of clarity).

The shortest Br···Br and O···Br distances in **1** are 5.839(1) [Br(2)···Br(2a)] and 5.814(3) Å [O(4)···Br(3b) and Br(3)···O(4c); symmetry codes: $b = x + 1/2, 3/2 - y, z + 1/2$; $c = x - 1/2, 3/2 - y, z - 1/2$], values which are similar to the corresponding ones in **2** [the shortest interionic Cl···Cl and O···Cl distances being 6.210(4) and 5.756(8) Å, respectively].[13]

3.2. Magnetic Properties of $(NBu_4)_2[ReX_4(ox)]$ [*X* = Br (1) and Cl (2)]. *3.2.1. Dc Study of 1.* Magnetic properties of **2** were investigated previously,[10a,13] and it was shown that they correspond to those of a magnetically isolated Re(IV) center ($S_{Re} = 3/2$ with $g_{//} = 1.78$ and $g_{\perp} = 1.89$) with a very large zfs, $|D| = 53$ cm^{-1}, where $2|D|$ is the energy gap between the $M_S = \pm 3/2$ and $\pm 1/2$ Kramers doublets resulting from the combined action of the second-order spin−orbit interaction and the tetragonal crystal field (in the case of a rhombic zfs tensor the gap is $2[D^2 + 3E^2]^{1/2}$).[10a]

The temperature dependence of the magnetic susceptibility of **1** is shown in Figure 3, where χ_M is the magnetic

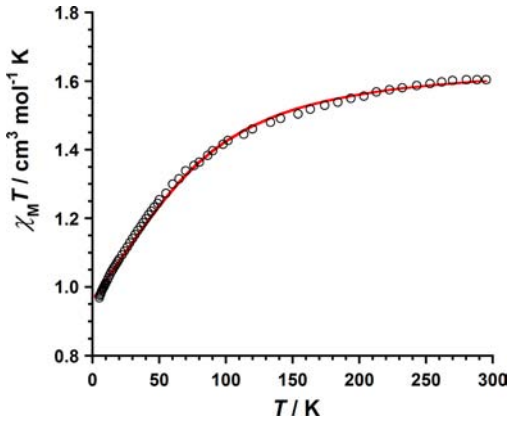

Figure 3. Thermal variation of the $\chi_M T$ product for **1**: (o) experimental; (—) best-fit curve generated by eq (1) (see text).

susceptibility per one Re(IV) ion. It follows the same pattern as that observed for **2** and other six-coordinate Re(IV) complexes.[10] At room temperature, $\chi_M T$ for **1** is 1.60 cm^3 mol^{-1} K, a value which is expected for a magnetically isolated Re(IV) center ($S_{Re} = 3/2$ with $g = 1.8-1.9$). Upon cooling, $\chi_M T$ decreases, first slowly and then faster, reaching a minimum value of ca. 0.97 cm^3 mol^{-1} K at 2.0 K. No maximum of χ_M is observed for **1** in the whole temperature range. The observed decrease of $\chi_M T$ is due to zfs effects of the six-coordinate Re(IV) ion, the intermolecular interactions being negligible because of the presence of the bulky organic cations.

Having these features in mind, the magnetic susceptibility data of **1** were analyzed by means of the standard spin Hamiltonian:

$$\mathcal{H} = D[\hat{S}_z^2 - S(S+1)/3] + g\beta_e(H_x\hat{S}_x + H_y\hat{S}_y + H_z\hat{S}_z) \quad (1)$$

where the first term accounts for the zfs of the Re(IV) center, and the second term corresponds to the Zeeman effect. In order to avoid overparameterization, an axial zfs tensor and isotropic *g* factor were assumed. Best least-squares fit parameters for **1** are $|D| = 73$ cm^{-1} and $g = 1.86$ with $F = 5.7 \times 10^{-5}$ {*F* is the agreement factor defined as $\Sigma[\phi_{obs}(i) - \phi_{calc}(i)]^2/\Sigma[\phi_{obs}(i)]^2$, ϕ being the physical magnitude to fit the $\chi_M T$ product}. The calculated curve for **1** (solid line in Figure 3) reproduces very well the magnetic data in the whole temperature range. The value of *D* obtained for **1** is somewhat greater than that previously reported for **2**. This feature suggests that the nature of the halide ligand modifies the anisotropy of the Re(IV) ion in the octahedral $[ReX_4(ox)]^{2-}$ entities [X = Br (**1**) and Cl (**2**)].[11c]

Magnetization (*M*) versus applied dc magnetic fields at different temperatures for **1** was carried out both on polycrystalline solid samples and on acetonitrile solutions (Figure 4). Both measurements match well, allowing one to discard intermolecular magnetic interactions that often occur in the rhenium(IV) complexes. This matching also confirms that the changes in the molecular geometry from solid to solution phases are not significant. The analysis of these measurements allowed us to estimate the values of the axial parameter *D* and the rhombicity factor *E*/*D* and also to determine the sign of *D*. A fit to the experimental magnetization curves of **1** was done using 30 orientations of the magnetic field whose projections on a sphere lead to equidistant points, to construct a powder pattern. A strong correlation between the values of the *g* factor and those of *D* and *E*/*D* was found. The experimental curves can therefore be properly reproduced with several sets of values for these parameters. The set we selected was the one which bore the strongest similarity to the magnetization result for *D* and to HFEPR for *E*/*D*: $g = 1.83$, $D = -62.6$ cm^{-1}, and $E/D = 0.19$ (in solution) and $g = 1.83$, $D = -62.6$ cm^{-1}, and $E/D = 0.22$ (in the solid state). The values of the agreement factor *F* (defined as above but ϕ being *M*) are 2.6×10^{-4} and $1.5 \times$

dx.doi.org/10.1021/ja403154z | J. Am. Chem. Soc. 2013, 135, 13737−13748

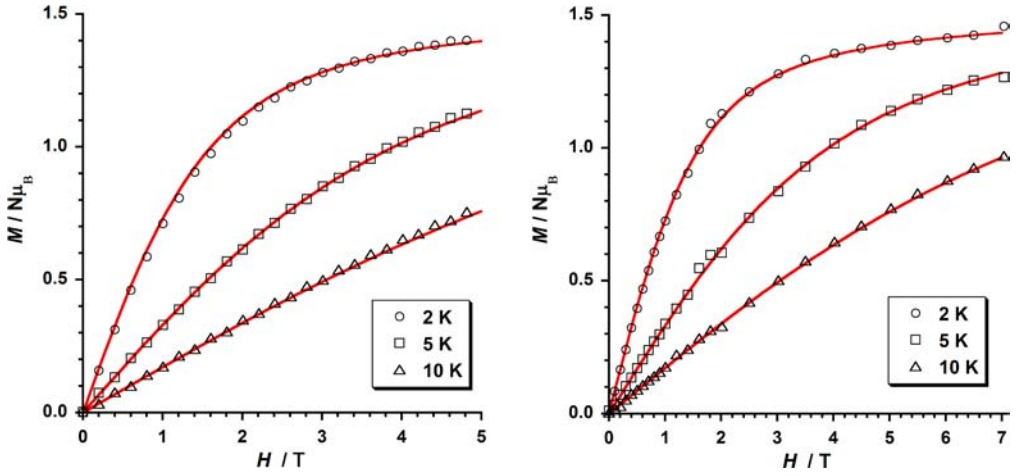

Figure 4. Field dependence of the magnetization at 2, 5, and 10 K for **1** (left) as the polycrystalline sample and (right) in the acetonitrile solution. The solid lines are the best-fit curves (see text).

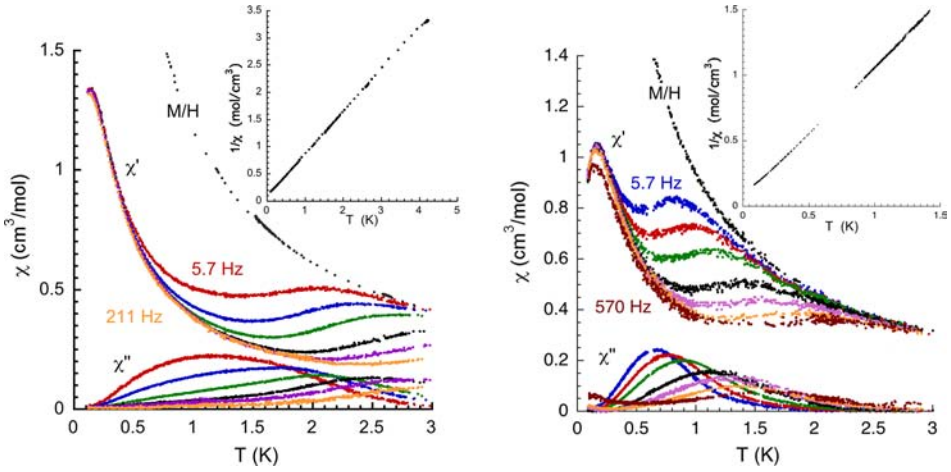

Figure 5. The frequency and temperature dependence of the real (χ_M') and imaginary (χ_M'') parts of the ac susceptibility vs temperature at various frequencies in a dc field of 2000 G. Also shown is the dc susceptibility M/H measured in a field of 500 G. The insets in the figures are plots of the inverse of the dc susceptibility vs T for compounds **1** (left) and **2** (right).

10^{-4}, respectively. We can simultaneously reproduce very well the experimental susceptibility and magnetizations curves from these values. The same process was also done imposing positive values for the D parameter, but this leads to poorer agreements with the experimental data. Finally, similar negative values for D were obtained from CAS calculations (see below) and, therefore, the possibility of positive values for D was rejected.

3.2.2. Ac Study of 1 and 2. Preliminary studies of the frequency-dependent ac susceptibility for compound **1** showed incipient out-of-phase signals under applied external magnetic fields (see Figure S1 of the Supporting Information), indicating the occurrence of slow relaxation of the magnetization reminiscent of a SMM behavior. No out-of-phase ac signals were observed in the lack of a dc magnetic field. Given that the maxima of the out-of-phase peaks would occur at temperatures lower than 2.0 K, we obtained rough values of these parameters by using the expression $\chi_M''/\chi_M' = 2\pi\nu\tau_o \exp(E^{\#}/k_BT)$ with experimental data from the χ_M''/χ_M' versus $1/T$ plot at a given frequency (see Figure S1 of the Supporting Information) and by assuming only a single relaxation time.[43] These rough values for τ_o and $E^{\#}$ are 10^{-6} s and 11 cm^{-1}, respectively. The χ_M'' versus χ_M' plots (Cole−Cole plots)[44] at different values of the temperatures and dc magnetic fields for **1** gave semicircles (Figure S2 of the Supporting Information) with small values of α (α = 0.15 − 0.25).

In order to get more precise information about the slow magnetic relaxation of compounds **1** and **2**, ac susceptibility measurements at lower temperatures (0.1−3.0 K) and under applied dc fields of 1000, 2000, and 5000 G were performed with a SQUID magnetometer equipped with a miniature dilution refrigerator (see Experimental Section). Figure 5 shows the real χ_M' and imaginary χ_M'' parts of the ac susceptibility versus the temperature for compounds **1** (left) and **2** (right) taken at various frequencies. These data were obtained by using a small ac field of 5 G and under a dc field of 2000 G. The dc susceptibility M/H measured in a field of 500 G is also shown. The insets in Figure 5 are plots of the inverse of the dc susceptibility versus T. These plots are nearly straight lines, with a very small negative intercept at the T axis, indicating the quasi absence of intermolecular interactions in these compounds. As seen in Figure 5, the peaks in χ_M'' shift to higher temperatures with increasing frequency. The real part χ_M' shows an anomaly in the vicinity of the peaks in χ_M'' but then continues to increase as the temperature is decreased for this dc field value.

dx.doi.org/10.1021/ja403154z | J. Am. Chem. Soc. 2013, 135, 13737−13748

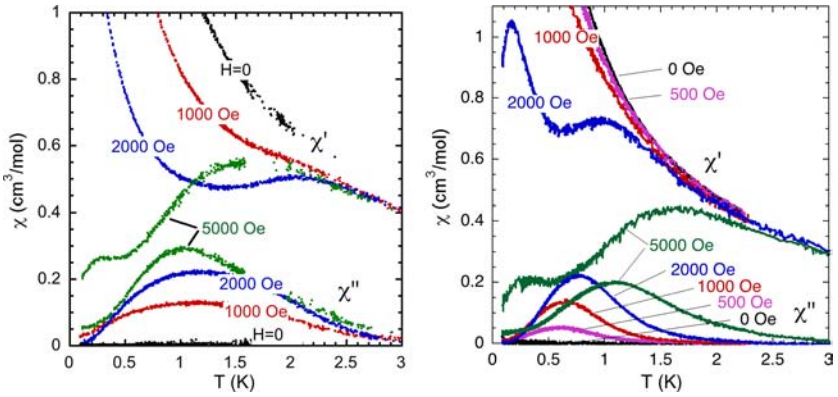

Figure 6. Field dependence of the ac susceptibility at a fixed frequency of 5.7 Hz for compounds **1** (left) and **2** (right).

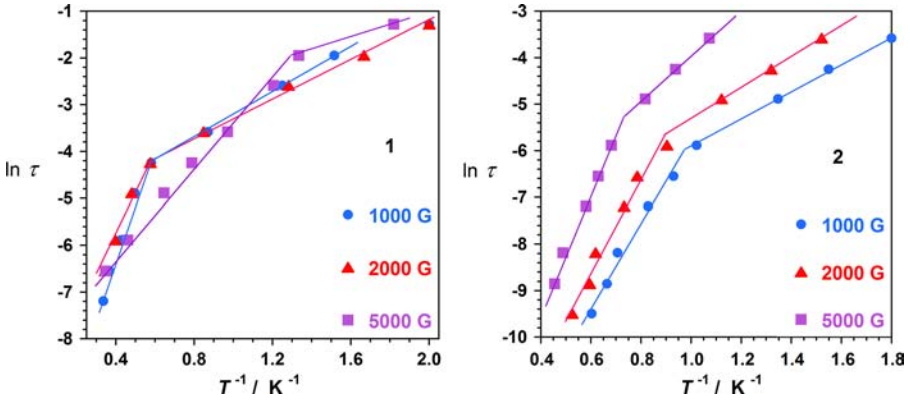

Figure 7. Logarithm of the effective relaxation time, $\tau = 1/2\pi\nu$ vs 1/T for compounds **1** and **2** derived from the maximum in χ_M'' by using the Arrhenius equation, $\ln \tau = \ln \tau_o + E^{\#}/k_BT$ for each regime under dc magnetic fields of 1000, 2000, and 5000 G. The values of τ_o and $E^{\#}$ obtained are given in Table 3.

Table 3. Values of T_c, τ_0, and $E^{\#}$ Obtained from the Arrhenius Plots for Different dc Applied Magnetic Fields (See Figure S7 of the Supporting Information)

H_{DC}	1000 G			2000 G			5000 G		
comp	T_c	$-\log \tau_0$	$E^{\#}$	T_c	$-\log \tau_0$	$E^{\#}$	T_c	$-\log \tau_0$	$E^{\#}$
1	1.7	5.1/2.4	9.6/1.5	1.7	4.7/2.3	8.5/1.4	0.8	3.5/1.6	3.2/1.0
2	1.0	6.4/3.9	6.3/2.1	1.1	6.7/3.6	7.8/2.3	1.4	6.3/3.9	8.8/3.6

The field dependence of the ac susceptibility at a fixed frequency of 5.7 Hz is shown in Figure 6 for both compounds. As can be seen, at zero applied dc field, no maximum of χ_M'' is detectable. However, when a dc field is applied, peaks become apparent. On the other hand, the dc field suppresses and distorts χ_M', and this effect is very pronounced at 5000 G. The distortion of χ_M' at high fields and low temperatures is due to the rapid approach to saturation as the temperature is decreased. The maxima in χ_M'' for compound **2** shift to higher temperatures with increasing the field for a given frequency. Curiously, the position of the peaks hardly change for compound **1**.

We can quantify the slowing down of the dynamics by associating the temperature of the maximum of the χ_M'' curves at a given frequency ν with an effective relaxation time $\tau = 1/2\pi\nu$. A plot of ln τ versus $1/T$ is shown in Figure 7 (Arrhenius plot) for both compounds at different applied dc fields. As one can see therein, two regimes occur for **1** and **2**, above and below the values of the temperature (T_c) shown in Table 3. The analysis of the data through the Arrhenius equation $\ln \tau = \ln \tau_o + E^{\#}/k_BT$ for each regime under dc magnetic fields of 1000, 2000, and 5000 G provides the values of τ_o and $E^{\#}$ given in Table 3. These values are similar to those observed in the preliminary study through the equation $\chi_M''/\chi_M' = 2\pi\nu\tau_o \exp(E^{\#}/k_BT)$ (see Figure S1 of the Supporting Information).

The values of the relaxation times for compound **2** are practically independent of the applied dc field, whereas the energy barrier slightly increases with the increasing field. Similar trends occur for compound **1** under applied dc fields of 1000 and 2000 G. However, a significant change occurs for this compound under an applied dc field of 5000 G. These features are common for the two regimes. The existence of two regimes in **1** and **2** can be attributed to the quantum tunneling effect of the magnetization (QTM) which would be operative in the low temperature region ($T < T_c$). Without an applied dc field, the relaxation is very fast, presumably due to resonant tunneling between the two components of the ground Kramers doublet. Applying a field lifts the degeneracy and suppresses the fast relaxation by tunneling. The values of τ_o and $E^{\#}$ reported here for **1** and **2** are in very good agreement with those found in the literature for polynuclear systems displaying fast resonant tunneling.[45]

dx.doi.org/10.1021/ja403154z | J. Am. Chem. Soc. 2013, 135, 13737−13748

3.2.3. HFEPR Study of 1 and 2. EPR being a standard method to investigate paramagnetic spin systems, we submitted **2** to conventional experiments at the Q band (34 GHz). The spectrum, obtained on a loose powder of **2** and shown in Figure S3 of the Supporting Information, is dominated by a single resonance at g_{eff} = 4.85 and is not helpful in terms of interpretation, although it shows a characteristic hyperfine sextet of lines with a splitting of about 49 mT, originating from the interaction of the nuclear spins of the two dominant isotopes of rhenium, ^{185}Re and ^{187}Re, both I = 5/2, with the electron spins, as observed before.[46] In order to obtain interpretable spectra, we carried out an HFEPR study at frequencies up to 640 GHz. We hoped to substantiate both the magnitude and sign of zfs in **1** and **2**, which are difficult to determine accurately from magnetic susceptibility measurements on powder samples.

Figure S4 of the Supporting Information shows HFEPR spectra of a loose powder of **2** at 20 K and 201.6 GHz. While the spectrum is dominated by the same feature at g_{eff} = 4.35 as in the Q band (see above), we noticed that the overall response varied between consecutive field sweeps, even though all the experimental parameters remained constant. The spectrum remains unchanged after six field sweeps. This is a signature of field torquing, which in the extreme case yields single-crystal-like spectra.[47] However, it was still not possible to attribute the single g_{eff} = 4.35 feature observed in the field-oriented sample to a particular transition within the S = 3/2 spin manifold. In order to understand HFEPR spectra of loose powder, we thus performed an experiment on an oriented single crystal.

Figure 8 (inset) shows an EPR spectrum of a single crystal of **2** at a fixed orientation, corresponding to 23 deg away from the crystallographic c axis, while rotating the crystal around the b axis at 20 K and 240 GHz. Two resonances are observed at this orientation, each showing the now-familiar hyperfine sextet. This is in agreement with the crystal structure, in which there are four $[ReCl_4(ox)]^{2-}$ complexes per unit cell, of which two are magnetically nonequivalent. The most relevant information was obtained from the angular dependence of these resonances, shown in the main part of Figure 8 (the hyperfine components were omitted for clarity in this plot). In particular, that dependence showed a narrow angular region for each of the two magnetically nonequivalent sublattices (around 30 and 150 deg, respectively), where the resonances go sharply off the magnetic field limit (12.5 T in this case). Simulations showed that for an S = 3/2 spin state, such an angular pattern is characteristic for the intra-Kramers resonance within the $|S, M_S\rangle$ = $|3/2, \pm 3/2\rangle$ Kramers doublet. Given that the experiment was conducted at low temperature (20 K), it proves that this doublet lies lower on the energy scale than its $|3/2, \pm 1/2\rangle$ equivalent. Accordingly, the zfs parameter D is negative for **2**. Another important conclusion obtained from simulations dealt with the fact that the nominally forbidden $\Delta M_S = \pm 3$ transition dominates the spectrum while the allowed $\Delta M_S = \pm 1$ resonance is not detectable at all. This is so because the mixing of the $|3/2, \pm 1/2\rangle$ and $|3/2, \pm 3/2\rangle$ Kramers doublet wave functions through the rhombic zfs parameter E makes both transitions almost equally probable, while the large negative D makes the $|3/2, \pm 1/2\rangle$ doublet depopulated at low temperatures. This is an indication that the rhombicity of the zfs tensor must be significant (E/D > 0.1 through simulations of intensities). Simulations of the angular dependence, as shown in Figure 8, showed that it is critically sensitive to E/D, while only weakly dependent on the g values. We obtained the best agreement between the simulations and experiment for E/D = 0.24. Furthermore, the angular dependence of the single-crystal resonances explains the powder spectrum shown in Figure S4 of the Supporting Information: the spectrum is indeed a quasi-single crystal one, with most of the crystallites oriented so that all the complexes are magnetically equivalent. This orientation corresponds to the crossing point of the angular dependencies of the two magnetically nonequivalent sublattices at 90 deg in Figure 8. Finally, the failure to observe any inter-Kramers transitions between the two Kramers doublets up to the highest available frequencies (640 GHz in our case), which in principle could make it possible to determine the zfs the way it was done in analogous S = 3/2 spin systems such as Co(II),[48] gives the lower bound for $|D|$ of 20 cm^{-1}, as determined by simulations. In other words, frequencies and fields available in our HFEPR setup do not allow determining the magnitude of the zfs in complex **2** but set the lower limit to it.

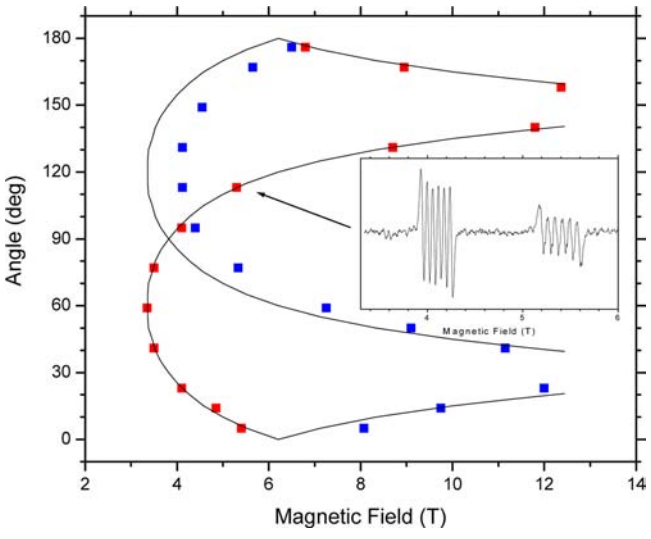

Figure 8. Inset: an HFEPR spectrum of a single crystal of **2** at the orientation denoted by the arrow. Frequency: 240 GHz; temperature: 20 K. Main plot: angular dependence of HFEPR resonances in the same conditions, represented by squares. For clarity, the center of each hyperfine sextet was taken as the resonance position; different colors denote magnetically nonequivalent sublattices. The crystal was rotated approximately about the b crystallographic axis; the rotation axis corresponded to a zfs principal axis of one of the sublattices but not exactly to the other due to a misalignment. The lines represent simulations using spin Hamiltonian parameters, as given in the text and in the caption of Figure 9.

To prevent the pervasive field-torquing in the powder sample of **2**, we pressed it into a pellet with *n*-eicosane. The resulting EPR spectrum at 10 K and 56 GHz is shown in Figure 9 (top) together with two simulations: the upper (blue) trace uses an "effective spin" S = 1/2 spin Hamiltonian, which has been an acknowledged way of dealing with high-spin systems for which the zfs far exceeds the EPR energy quantum. The lowest (red) trace, to the contrary, uses the true S = 3/2 Hamiltonian, and yields results far superior to the effective-spin formalism in terms of line shape, and intensities of the particular turning points in the powder spectrum. Indeed, the agreement between the simulation and experiment in the latter case is nothing short of textbook quality. Increasing the EPR frequency (not shown) results in a broadening of the individual hyperfine components,

dx.doi.org/10.1021/ja403154z | J. Am. Chem. Soc. 2013, 135, 13737−13748

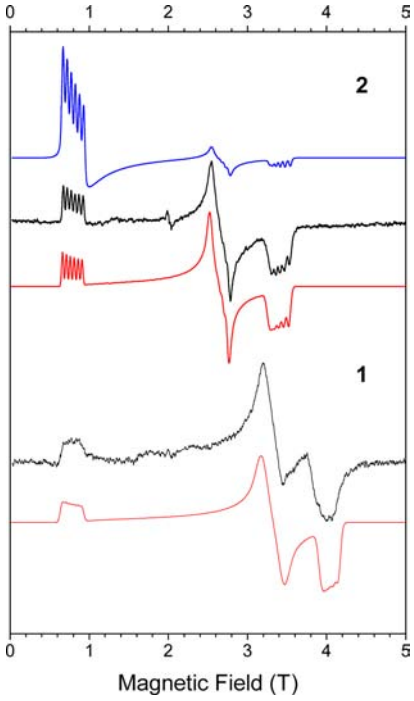

Figure 9. (Top) An EPR spectrum of complex **2** as a pellet (black trace). Frequency: 56 GHz, temperature: 10 K. The blue trace was simulated using an effective spin Hamiltonian, with the parameters: S = 1/2, g_{eff} = [1.17, 1.50, 5.0], I = 5/2, A = [37, 48, 48] × 10^{-3} cm^{-1}. The red trace was simulated using a true S = 3/2 spin Hamiltonian, with the parameters: D = −53 cm^{-1}, E/D = 0.26, g = [1.89, 1.89, 1.80], I = 5/2, A = [36, 45, 41] × 10^{-3} cm^{-1}, and single-crystal line width [20, 17.5, 40] mT. The weak signal at 2 T in the experimental spectrum is due to a Mn(II) impurity and not simulated. (Bottom) An analogous spectrum of complex **1** in the same experimental conditions. Simulation parameters: S = 3/2, D = −73 cm^{-1}, E/D = 0.205, g = [1.89, 1.90, 1.77], I = 5/2, A = 41 × 10^{-3} cm^{-1} (isotropic), and single-crystal line width 40 mT (isotropic).

this leads to smearing out of the hyperfine structure, presumably by such effects as g strain.[49] This can be observed in Figure 9 (bottom), which shows the analogous spectrum of complex **1** and its simulation. When simulating spectra for complex **1**, we used the magnetometry-determined magnitude of $|D|$ = 73 cm^{-1}, similarly to complex **2**, while varying all other spin Hamiltonian parameters, which turn out to be similar to those of complex **2**: the negative sign of D, the somewhat lower rhombicity factor E/D = 0.205, and almost identical g values. The notable difference was the single-crystal line width that had to be assumed in the simulations, larger by a factor of about two than that of complex **2**. This accounts for the only partially resolved hyperfine components in the spectra.

In brief, the HFEPR experiment, although not able to deliver the magnitude of D for either complex due to insufficient operating frequency, was able to obtain (a) the negative sign of D, (b) the high rhombicity factors (0.20 − 0.25) of the zfs tensors, and (c) confirm the g values for both complexes.

3.3. CAS- and DFT-Type Calculations. The zfs of transition metal complexes has been extensively studied from a theoretical perspective due to the interest in the design of new single-molecule magnets (SMMs) and more recently of mononuclear SMMs that can be used in the nanotechnology field.[9d] Quantum chemistry allows us to establish a connection between molecular geometry and zfs parameters through electronic aspects. In this sense, so far, a post-Hartree−Fock method, Complete Active Space (CAS), and other computational methodologies based on the Density Functional Theory (DFT) have been used.[28,50−62] Although good qualitative results have been obtained by using both of them, more accurate D and E values have been procured by the former one. In this work, the two methodologies have been used and compared.

The Re(IV) ion displays a high-spin d^3 electronic configuration, having the three unpaired electrons placed in three different d orbitals. In an ideal octahedral ligand field, these magnetic orbitals correspond to degenerate t_{2g} orbitals ($^4A_{2g}$). These electrons can be promoted to the e_g orbitals, generating six quartet excited states ($^4T_{2g}$ and $^4T_{1g}$) whose energies relative to the ground state are equal or slightly higher than the ligand-field splitting parameter. The other three excited states ($^4T_{1g}$) generated by promotion of two electrons from t_{2g} to e_g orbitals can be found at higher-enough energy. In a C_{2v} symmetry, closer to the experimental one, these grouped states are split. On the other hand, two d electrons can be paired. In such a case, only one d orbital is magnetic and low-energy doublet excited states can be built (^2E_g and $^2T_{1g}$), according to the placement of the paired and unpaired electrons. The promotion of paired or unpaired electrons from t_{2g} to e_g orbitals leads to other excited states placed at higher energies and showing small influence on the ground spin state. Also, other doublet excited states can be generated with all electrons unpaired, but they are far from the ground state.

Table 4. Values of D (in cm^{-1}), Their Spin−Spin (D_{SS}, in cm^{-1}), Spin−Orbit (D_{SO}, in cm^{-1}) (From Quartet [D_Q] and Doublet [D_D]) Contributions and E/D obtained from *CAS* and *DF* Studies Using the *ZORA* Formalism and without the Inclusion of Electronic Effects of the Molecular Surrounding

compound	methodology*	D_{SS}	D_{SO}	D_Q	D_D	D	E/D
1							
	CAS {10,10}	−0.03	−55.41	–	–	−55.44	0.19
	CAS {10,20}	−0.03	−53.41	–	–	−53.44	0.23
	PBE	−0.03	−64.13	−5.46	−61.97	−64.16	0.30
	BLYP	−0.03	−70.62	−5.42	−68.63	−70.65	0.33
2							
	CAS {10,10}	−0.03	−60.30	–	–	−60.33	0.22
	CAS {10,20}	−0.03	−61.11	–	–	−61.14	0.22
	PBE	−0.04	−67.08	−5.75	−65.62	−67.12	0.33
	BLYP	−0.03	−73.47	−5.81	−72.31	−73.50	0.32

*CAS{n,m}: n and m quartet and doublet states have been used in the estimation of D and E/D values.

dx.doi.org/10.1021/ja403154z | J. Am. Chem. Soc. 2013, 135, 13737−13748

Each one of the quartet and doublet excited states can mix with the spin ground state through spin−orbit coupling, leading to a splitting of the M_S states of the ground state (i.e., zfs). Ten quartet and twenty doublet states arise from three electrons and five *d* orbitals. One of them, a quartet state is the ground state and the remaining ones are excited states. Evidently, when the energy gap between the ground and excited states is large, the mixing between them will be weak and the contribution to the zfs parameters will be correspondingly small. On the other hand, the calculations become less expensive and time-consuming by restricting the size of active space or the number of excited states used. We have thus used an active space that takes into account the five d orbitals. Among all states that can be generated within this active space, (10, 10) and (10, 20) sets (quartet, doublet) have been chosen to compare their influence on the zfs. Although there are differences between the values of the *D* parameter obtained in each case, they are not important relative to the large magnitude of *D*. However, significant effects can be observed on the *E* parameter and, consequently, on the *E*/*D* ratio. The use of a (10, 20) full set leads to the same order of magnitude for the *E*/*D* ratio for **1** and **2**, being closer to the values extracted from the HFEPR spectra (see Table 4) than those in the case of the smaller set. No significant changes of the values of *D* and *E*/*D* are found when electronic effects induced by the acetonitrile as solvent are included (see Table S1 of the Supporting Information). The inclusion of relativistic effects by using the *ZORA* or *DHK* formalisms do not cause remarkable differences in the values of *D* and *E*/*D* (see Table S1 of the Supporting Information). Figure S5 of the Supporting Information shows how the *D* tensor is oriented on the complex **2**, being its *z* axis placed on the molecular *x* axis. Comparisons with HFEPR experimental results were possible concerning the *E*/*D* ratio, but they were not done regarding the *D* parameter because HFEPR only allowed us to establish a negative sign and estimate the absolute value as larger than 20 cm^{-1} for this parameter. Nevertheless, a comparison with the magnetic results could be made and the theoretical values [ca. −61 (**1**) and −53 cm^{-1} (**2**)] are in agreement with the experimental evidence. These results validate the proposed sign for *D* from the magnetic susceptibility and magnetization data [ca. −63 (**1**) and −53 cm^{-1} (**2**)]. However, from an optimized molecular geometry of **2** using the *PBE* functional and Gaussian09 program, a too large negative *D* value (−95.9 cm^{-1} from a *CAS* calculation) was obtained. Although the metal−ligand bond lengths from the optimized geometries are longer than those observed in the crystal structure (Table S5 of the Supporting Information), it is a typical feature of the *DF* calculations that they overestimate the bond lengths, leading to a weakening to the ligand field and, in consequence, to a situation closer to the free ion with larger *D* values. Perhaps a study in the solid state, where the pressure effects from the network are also considered, can provide more accurate metal−ligand bond lengths and ligand field values. A study in that respect is in progress.

In many instances D_{SS}, the spin−spin contribution to the *D* parameter is smaller than D_{SO}, which is the contribution from the spin−orbit coupling but not negligible. This is not the case here, whereas our calculations result in D_{SS}, much smaller than D_{SO} (see Table 4). Therefore, the axial magnetic anisotropy is only composed of the spin−orbit coupling between the ground and excited states. Similar results are found from *DFT* calculations, but the *D* and *E*/*D* values obtained through DFT are larger than those procured from CAS calculations, independently of the functional used (*PBE* or *BLYP*). The spin−orbit contribution to the *D* parameter can be separated into two contributions, originating from the quartet (D_Q) and doublet (D_D) states. The closest excited quartet states are placed at an energy above that due to the ligand field splitting [first excited state at 29002.2 (**1**) and 29434.3 cm^{-1} (**2**) from CAS calculations], since these involve the promotion of one electron at least from a t_{2g} to one e_g orbital; however, because of the large ligand field of the Re(IV) ion, some $(t_{2g})^3$ doublet excited states are also close to the ground state [first excited triplet state at 12361.2 (**1**) and 12359.0 cm^{-1} (**2**) from CAS calculations]. Thus, DFT and CAS results show that although the contribution from the excited quartet states are significant, the presence of these nearby doublet excited states, together with the large value of the spin−orbit coupling constant (λ about 1000 cm^{-1}), is responsible for the very large value of *D*.

The lack of ac response in the absence of a dc field can be understood by a fast relaxation through tunneling effects, which are more probable in mononuclear than in polynuclear complexes. When a dc field is applied, the ground M_S states are not degenerate anymore and the relaxation by tunneling effects is prevented. Therefore, the blocking temperature is higher when the applied dc field increases. However, the observed blocking temperatures, and also the values of the activation energy, are lower than those calculated theoretically. The certainty of the theoretically calculated values is irrefutable because of the good agreement found between the values of *D* and *E*/*D* obtained from HFEPR, magnetization measurements, and theoretical calculations. The inconsistency between the *D* values and the blocking temperatures for **1** and **2** requires therefore some consideration. A possible answer based on a different magnetic anisotropy of the crystal caused by a relative misorientation between the molecular entities in the crystal is rejected because the molecular anisotropy axes are pretty much collinear. On the other hand, it is known that the geometry does not remain rigid, even at low temperature. Although it is possible to determine the geometry of a molecule in nature, it only corresponds to an average geometry but is not fixed as their atoms move because of the vibrational modes of the molecule. These geometrical changes increase with temperature and even if they are not very large at low temperatures, they can be crucial as far as the order of energies of the excited states are concerned. In fact, DF calculations predict the presence of oxalate bending from the basal plane ReO_2Cl_2, as a fluttering, at lower energies. This situation is exemplified by the doublet excited states of Re(IV) complexes that are only distinguished by the different population of the very close t_{2g} orbitals. These excited doublet states contribute to the *D* parameter in a different way (i.e., either favoring positive or negatives values of *D*). The sum and level of compensation of all these contributions provides the sign and magnitude of the *D* parameter. In a system where the excited states are very close, their order and energy gap can significantly change the value of *D* and this change can occur by modification of the ligand-field strength induced by small adjustments in the molecular geometry. Thus, a short molecular dynamics on the optimized molecular geometry of **2** in solution has been done at 10 K using the vibrational modes to calculate the initial velocities and trajectories. An evaluation of the *D* parameter from CAS calculations was done for 1000 molecular geometries extracted from the molecular dynamics simulation. A probability distribution of the values of *D* shown in Figure 10 shows a wide range of these values where even its mean is quite high.

dx.doi.org/10.1021/ja403154z | J. Am. Chem. Soc. 2013, 135, 13737−13748

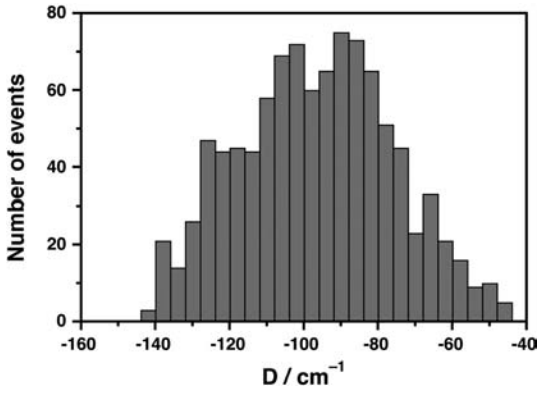

Figure 10. Distribution of the probability for the D values obtained from the structure of **2** extracted through a molecular dynamic simulation at 10 K.

The distribution is close to a Gaussian curve centered at D around −95 cm^{-1}, which is a larger value than that found from the experimental geometry but similar to the one found for the optimized geometry (−95.9 cm^{-1}). As mentioned above, more relaxed molecular geometries with larger metal−ligand bond lengths usually found by DF methods are responsible for the weaker ligand field and the higher magnetic anisotropies (Table S5 and Figure S6 of the Supporting Information). One can see in Figure 10 that values in the range of −40 and −140 cm^{-1} (−90 ± 50) can be reached. It is thus reasonable to assume that some molecular geometries with low D values providing low activation energies and blocking temperatures could be involved. In this sense, a decrease of ca. 50 cm^{-1} of the D values determined for **1** and **2** could afford values of D as low as those causing the energy barrier estimated from the ac measurements. A deeper study of this possibility in molecular and solid models is in progress.

4. CONCLUSIONS

In summary, **1** and **2** are the first reported examples of 5d-based mononuclear single-molecule magnets. They exhibit a fast relaxation of the magnetization due to quantum tunneling effects (QTM) in the absence of an applied dc magnetic field. These QTM effects disappear in the presence of an applied dc field and a slow magnetic relaxation takes place. The main question is to understand the mechanism of that relaxation. An energy barrier of about 10 cm^{-1} is estimated for **1** and **2** from the experimental data. However, the energy gap between the ground state and the lowest excited spin level for these molecules is ca. 110−130 cm^{-1}, that is one order of magnitude greater than the energy barrier. It is postulated that vibrational levels involving molecular distortions may give rise to D values closer to those responsible for the energy barrier. Theoretical studies of these vibrational molecular distortions with low D values and a half-life long enough to relax are under investigation.

■ ASSOCIATED CONTENT

Ⓢ Supporting Information

X-ray structural information for **1** was deposited with the Cambridge Crystallographic Data Centre, 12 Union Road, Cambridge CB2 1EZ, UK. These data can be obtained free of charge via the Internet at http://www.ccdc.cam.ac.uk/conts/retrieving.html, by fax: +44 1223 336 033, or by e-mail: deposit@ccdc.cam.ac.uk. The CCDC number is 854108. Figures S1−S6 and Tables S1−S5. This material is available free of charge via the Internet at http://pubs.acs.org.

■ AUTHOR INFORMATION

Corresponding Author

f.jose.martinez@uv.es; juan.faus@uv.es; krzystek@magnet.fsu.edu

Present Address

[¶]Hamilton College, Clinton, New York 13323.

Notes

The authors declare no competing financial interest.

■ ACKNOWLEDGMENTS

We thank Dr. Graeme Hanson for his help in implementing the XSophe EPR simulation program, and Dr. Andrew Ozarowski for his simulation program SPIN. Financial support from the Spanish Ministerio de Ciencia e Innovación (Projets Consolider-Ingenio in Molecular Nanoscience CSD2007-00010 and CTQ-2010-15364), the Generalitat Valenciana (Project PROMETEO/2009/108), and the Italian Ministero dell'Istruzione, dell'Università e della Ricerca Scientifica, through the Centro di Eccellenza CEMIF.CAL (Grant CLAB01TYEF) is gratefully acknowledged. HFEPR studies were supported by the NHMFL, which is funded by the NSF through a Cooperative Agreement DMR 1157490, the State of Florida, and the DOE. J.K. acknowledges the University of Valencia for a Visiting Professor fellowship.

■ REFERENCES

(1) (a) Sessoli, R.; Gatteschi, D. *Angew. Chem., Int. Ed.* **2003**, *42*, 268. (b) Gatteschi, D.; Sessoli, R.; Villain, J. *Molecular Nanomagnets*; Oxford University Press: Oxford, 2006. (c) Brechin, E. K.; Aromí, G. *Struct. Bonding (Berlin, Ger.)* **2006**, *122*, 1 and references therein.

(2) (a) Leuenberger, M. N.; Loss, D. *Nature* **2001**, *410*, 789. (b) Wernsdorfer, W.; Aliaga-Acalde, N.; Hendrickson, D. N.; Christou, G. *Nature* **2002**, *416*, 406. (c) Hill, S.; Edwards, R. S.; Aliaga-Acalde, N.; Christou, G. *Science* **2003**, *302*, 1015. (d) Tejada, J.; Chudnovsky, E. M.; Del Barco, E.; Hernandez, J. M.; Spiller, T. P. *Nanotechnology* **2001**, *12*, 181. (e) Affronte, M.; Casson, I.; Evangelisti, M.; Candini, A.; Carretta, S.; Muryn, C. A.; Teat, S. J.; Timco, G. A.; Wernsdorfer, W.; Winpenny, R. E. P. *Angew. Chem., Int. Ed.* **2005**, *44*, 6496. (f) Lehmann, J.; Gaita-Ariño, A.; Coronado, E.; Loss, D. *Nat. Nanotechnol.* **2007**, *2*, 312.

(3) Bogani, L.; Wernsdorfer, W. *Nat. Nanotechnol.* **2008**, *7*, 179.

(4) (a) Milios, C. J.; Raptopoulou, C. P.; Terzis, A.; Lloret, F.; Vicente, R.; Perlepes, S. P.; Escuer, A. *Angew. Chem., Int. Ed.* **2004**, *43*, 210. (b) Milios, C. J.; Vinslava, A.; Wood, P. A.; Parsons, S.; Wernsdorfer, W.; Christou, G.; Perlepes, S. P.; Brechin, E. K. *J. Am. Chem. Soc.* **2007**, *129*, 8. (c) Milios, C. J.; Vinslava, A.; Wernsdorfer, W.; Moggach, S.; Parsons, S.; Perlepes, S. P.; Christou, G.; Brechin, E. K. *J. Am. Chem. Soc.* **2007**, *129*, 2754. (d) Milios, C. J.; Vinslava, A.; Wernsdorfer, W.; Prescimone, A.; Wood, P. A.; Parsons, S.; Perlepes, S. P; Christou, G.; Brechin, E. K. *J. Am. Chem. Soc.* **2007**, *129*, 6547. (e) Milios, C. J.; Inglis, R.; Bagai, R.; Wernsdorfer, W.; Collins, A.; Moggach, S.; Parsons, S.; Perlepes, S. P.; Christou, G.; Brechin, E. K. *Chem. Commun.* **2007**, 3476. (f) Milios, C. J.; Inglis, R.; Vinslava, A.; Bagai, R.; Wernsdorfer, W.; Parsons, S.; Perlepes, S. P.; Christou, G.; Brechin, E. K. *J. Am. Chem. Soc.* **2007**, *129*, 12505. (g) Milios, C. J.; Piligkos, S.; Brechin, E. K. *Dalton Trans.* **2008**, 1809. (h) Datta, S.; Bolin, E.; Inglis, R.; Milios, C. J.; Brechin, E. K.; Hill, S. *Polyhedron* **2009**, *28*, 1788. (i) Inglis, R.; Jones, L. F.; Milios, C. J.; Datta, S.; Collins, A.; Parsons, S.; Wernsdorfer, W.; Hill, S.; Perlepes, S. P.; Piligkos, S.; Brechin, E. K. *Dalton Trans.* **2009**, 3403. (j) Tomsa, A.-R.; Martínez-Lillo, J.; Li, Y.; Chamoreau, L.-M.; Boubekeur, K.; Farias, F.; Novak, M. A.; Cremades, E.; Ruiz, E.; Proust, A.; Verdaguer, M.;

Gouzerh, P. *Chem. Commun.* **2010**, *46*, 5106. (k) Martínez-Lillo, J.; Tomsa, A.-R.; Li, Y.; Chamoreau, L.-M.; Cremades, E.; Ruiz, E.; Barra, A.-L.; Proust, A.; Verdaguer, M.; Gouzerh, P. *Dalton Trans.* **2012**, *41*, 13668. (l) Martínez-Lillo, J.; Chamoreau, L.-M.; Proust, A.; Verdaguer, M.; Gouzerh, P. *C. R. Chimie* **2012**, *15*, 889.

(5) (a) Ishikawa, N.; Sugita, M.; Ishikawa, T.; Koshihara, S.-Y.; Kaizu, Y. *J. Am. Chem. Soc.* **2003**, *125*, 8694. (b) Ishikawa, N.; Sugita, M.; Ishikawa, T.; Koshihara, S.; Kaizu, Y. *J. Phys. Chem. B* **2004**, *108*, 11265. (c) Ishikawa, N.; Sugita, M.; Wernsdorfer, W. *Angew. Chem., Int. Ed.* **2005**, *44*, 2931. (d) Ishikawa, N.; Mizuno, Y.; Takamatsu, S.; Ishikawa, T.; Koshihara, S.-Y. *Inorg. Chem.* **2008**, *47*, 10217.

(6) (a) AlDamen, M. A.; Clemente-Juan, J. M.; Coronado, E.; Martí-Gastaldo, C.; Gaita-Ariño, A. *J. Am. Chem. Soc.* **2008**, *130*, 8874. (b) AlDamen, M. A.; Cardona-Serra, S.; Clemente-Juan, J. M.; Coronado, E.; Gaita-Ariño, A.; Martí-Gastaldo, C.; Luis, F.; Montero, O. *Inorg. Chem.* **2009**, *48*, 3467. (c) Baldovi, J. J.; Cardona-Serra, S.; Clemente-Juan, J. M.; Coronado, E.; Gaita-Ariño, A.; Palii, A. *Inorg. Chem.* **2012**, *51*, 12565. (d) Li, D.-P; Wang, T.-W.; Li, C.-H.; Liu, D.-S.; Li, Y.-Z.; You, X.-Z. *Chem. Commun.* **2010**, *46*, 2929. (e) Jiang, S.-D.; Wang, B.-W.; Sun, H.-L.; Wang, Z.-M.; Gao, S. *J. Am. Chem. Soc.* **2011**, *133*, 4730. (f) Rinehart, J. D.; Long, J. R. *Chem. Sci.* **2011**, *2*, 2078.

(7) (a) Rinehart, J. D.; Long, J. R. *J. Am. Chem. Soc.* **2009**, *131*, 12558. (b) Rinehart, J. D.; Meihaus, K. R.; Long, J. R. *J. Am. Chem. Soc.* **2010**, *132*, 7572. (c) Antunes, M. A.; Pereira, L. C. J.; Santos, I. C.; Mazzanti, M.; Marçalo, J.; Almeida, M. *Inorg. Chem.* **2011**, *50*, 9915.

(8) (a) Zadrozny, J. M.; Xiao, D. J.; Atanasov, M.; Long, G. J.; Grandjean, F.; Neese, F.; Long, J. R. *Nat. Chem.* **2013**, *5*, 577. (b) Freedman, D. E.; Harman, W. H.; Harris, T. D.; Long, G. J.; Chang, C. J.; Long, J. R. *J. Am. Chem. Soc.* **2010**, *132*, 1224. (c) Harman, W. H.; Harris, T. D.; Freedman, D. E.; Fong, H.; Chang, A.; Rinehart, J. D.; Ozarowski, A.; Sougrati, M. T.; Grandjean, F.; Long, G. J.; Long, J. R.; Chang, C. J. *J. Am. Chem. Soc.* **2010**, *132*, 18115. (d) Weismann, D.; Sun, Y.; Lan, Y.; Wolmershäuser, G.; Powell, A. K.; Sitzmann, H. *Chem.—Eur. J.* **2011**, *17*, 4700. (e) Lin, P.-H.; Smythe, N. C.; Gorelsky, S. I.; Maguire, S.; Henson, N. J.; Korobkov, I.; Scott, B. L.; Gordon, J. C.; Baker, R. T.; Murugesu, M. *J. Am. Chem. Soc.* **2011**, *133*, 15806. (f) Mossin, S.; Tran, B.-L.; Adhikari, D.; Pink, M.; Heinemann, F. W.; Sutter, J.; Szilagyi, R. K.; Meyer, K.; Mindiola, D. J. *J. Am. Chem. Soc.* **2012**, *134*, 13651.

(9) (a) Zadrozny, J. M.; Long, J. R. *J. Am. Chem. Soc.* **2011**, *133*, 20732. (b) Jurca, T.; Farghal, A.; Lin, P.-H.; Korobkov, I.; Murugesu, M.; Richarson, D. S. *J. Am. Chem. Soc.* **2011**, *133*, 15814. (c) Zadrozny, J. M.; Liu, J.; Piro, N. A.; Chang, C. J.; Hill, S.; Long, J. R. *Chem. Commun.* **2012**, *48*, 3927. (d) Vallejo, J.; Castro, I.; Ruiz-García, R.; Cano, J.; Julve, M.; Lloret, F.; De Munno, G.; Wernsdorfer, W.; Pardo, E. *J. Am. Chem. Soc.* **2012**, *134*, 15704. (e) Colacio, E.; Ruiz, J.; Ruiz, E.; Cremades, E.; Krzystek, J.; Carretta, S.; Cano, J.; Guidi, T.; Wernsdorfer, W.; Brechin, E. K. *Angew. Chem. Int. Ed.* **2013**, *52*, 9130.

(10) (a) Chiozzone, R.; González, R.; Kremer, C.; De Munno, G.; Cano, J.; Lloret, F.; Julve, M.; Faus, J. *Inorg. Chem.* **1999**, *38*, 4745. (b) Chiozzone, R.; González, R.; Kremer, C.; De Munno, G.; Armentano, D.; Cano, J.; Lloret, F.; Julve, M.; Faus, J. *Inorg. Chem.* **2001**, *40*, 4242. (c) Chiozzone, R.; González, R.; Kremer, C.; De Munno, G.; Armentano, D.; Lloret, F.; Julve, M.; Faus, J. *Inorg. Chem.* **2003**, *42*, 1064. (d) Tomkiewicz, A.; Mroziński, J.; Brüdgam, I.; Hartl, H. *Eur. J. Inorg. Chem.* **2005**, 1787. (e) Tomkiewicz, A.; Mroziński, J.; Korybut-Daszkiewcz, B.; Brüdgam, I.; Hartl, H. *Inorg. Chim. Acta* **2005**, *358*, 2135. (f) Martínez-Lillo, J.; Armentano, D.; De Munno, G.; Wernsdorfer, W.; Julve, M.; Lloret, F.; Faus, J. *J. Am. Chem. Soc.* **2006**, *128*, 14218. (g) Martínez-Lillo, J.; Delgado, F. S.; Ruiz-Pérez, C.; Lloret, F.; Julve, M.; Faus, J. *Inorg. Chem.* **2007**, *46*, 3523. (h) Martínez-Lillo, J.; Armentano, D.; De Munno, G.; Lloret, F.; Julve, M.; Faus, J. *Dalton Trans.* **2008**, 40. (i) Martínez-Lillo, J.; Armentano, D.; De Munno, G.; Wernsdorfer, W.; Clemente-Juan, J. M.; Krzystek, J.; Lloret, F.; Julve, M.; Faus, J. *Inorg. Chem.* **2009**, *48*, 3027. (j) Martínez-Lillo, J.; Armentano, D.; De Munno, G.; Lloret, F.; Julve, M.; Faus, J. *Dalton Trans.* **2011**, *40*, 4818. (k) Martínez-Lillo, J.; Cañadillas-Delgado, L.; Cano, J.; Lloret, F.; Julve, M.; Faus, J. *Chem. Commun.* **2012**, *48*, 9242. (l) Martínez-Lillo, J.; Armentano, D.; De Munno, G.; Julve, M.; Lloret, F.; Faus, J. *Dalton Trans.* **2013**, *42*, 1687.

(11) (a) Chiozzone, R.; Cuevas, A.; González, R.; Kremer, C.; Armentano, D.; De Munno, G.; Faus, J. *Inorg. Chim. Acta* **2006**, *359*, 2194. (b) Chiozzone, R.; González, R.; Kremer, C.; Armentano, D.; De Munno, G.; Julve, M.; Lloret, F. *Inorg. Chim. Acta* **2011**, *370*, 394. (c) Martínez-Lillo, J.; Mastropietro, T. F.; De Munno, G.; Lloret, F.; Julve, M.; Faus, J. *Inorg. Chem.* **2011**, *50*, 5731.

(12) Harris, T. D.; Bennett, M. V.; Clérac, R.; Long, J. R. *J. Am. Chem. Soc.* **2010**, *132*, 3980.

(13) Tomkiewicz, A.; Bartczak, T. J.; Kruszyński, R.; Mroziński, J. *J. Mol. Struct.* **2001**, *595*, 225.

(14) Morley, G. W.; Brunel, L. C.; van Tol, J. *Rev. Sci. Instrum.* **2008**, *79*, 064703.

(15) Hassan, A. K.; Pardi, L. A.; Krzystek, J.; Sienkiewicz, A.; Goy, P.; Rohrer, M.; Brunel, L. C. *J. Magn. Reson.* **2000**, *142*, 300.

(16) Neese, F. *WIREs Computational Molecular Science* **2012**, *2*, 73.

(17) Schafer, A.; Huber, C.; Ahlrichs, R. *J. Chem. Phys.* **1994**, *100*, 5829.

(18) Schafer, A.; Horn, H.; Ahlrichs, R. *J. Chem. Phys.* **1992**, *97*, 2571.

(19) Kendall, R. A.; Fruchtl, H. A. *Theor. Chem. Acc.* **1997**, *97*, 158.

(20) Eichkorn, K.; Treutler, O.; Ohm, H.; Haser, M.; Ahlrichs, R. *Chem. Phys. Lett.* **1995**, *240*, 283.

(21) Eichkorn, K.; Treutler, O.; Ohm, H.; Haser, M.; Ahlrichs, R. *Chem. Phys. Lett.* **1995**, *242*, 652.

(22) Eichkorn, K.; Weigend, F.; Treutler, O.; Ahlrichs, R. *Theor. Chem. Acc.* **1997**, *97*, 119.

(23) Perdew, J. P.; Burke, K.; Enrzerhof, M. *Phys. Rev. Lett.* **1996**, *77*, 3865.

(24) Perdew, J. P.; Burke, K.; Enrzerhof, M. *Phys. Rev. Lett.* **1997**, *78*, 1396.

(25) Lee, C. T.; Yang, W. T.; Parr, R. G. *Phys. Rev. B* **1988**, *37*, 785.

(26) Becke, A. D. *Phys. Rev. A* **1988**, *38*, 3098.

(27) Klamt, A.; Schüürmann, G. *J. Chem. Soc., Perkin Trans. 2* **1993**, 799.

(28) Neese, F. *J. Am. Chem. Soc.* **2006**, *128*, 10213.

(29) Douglas, M.; Kroll, N. M. *Ann. Phys-New York* **1974**, *82*, 89.

(30) Hess, B. A. *Phys. Rev. A* **1985**, *32*, 756.

(31) Chang, C.; Pelissier, M.; Durand, P. *Phys. Scr.* **1986**, *34*, 394.

(32) Li, X. S.; Millan, J. M.; Schlegel, H. B. *J. Chem. Phys.* **2000**, *113*, 10062.

(33) Schlegel, H. B.; Millam, J. M.; Bakken, V.; Hase, W. L. *Abstr. Pap., Jt. Conf.—Chem. Inst. Can. Am. Chem. Soc.* **2000**, *219*, U350.

(34) Hay, P. J.; Wadt, W. R. *J. Chem. Phys.* **1985**, *82*, 270.

(35) Hay, P. J.; Wadt, W. R. *J. Chem. Phys.* **1985**, *82*, 229.

(36) Wadt, W. R.; Hay, P. J. *J. Chem. Phys.* **1985**, *82*, 284.

(37) Hu, X. C.; Hase, W. L.; Pirraglia, T. J. *Comput. Chem.* **1991**, *12*, 1014.

(38) Tomasi, J.; Mennucci, B.; Cammi, R. *Chem. Rev.* **2005**, *105*, 2999.

(39) *SAINT*, version 6.45; Bruker Analytical X-ray Systems: Madison, WI, 2003.

(40) Sheldrick, G. M. *SADABS Program for Absorption Correction*, version 2.10; Analytical X-ray Systems: Madison, WI, 2003.

(41) *SHELXTL*; Bruker Analytical X-ray Instruments: Madison, WI, 1998.

(42) Nardelli, M. *J. Appl. Crystallogr.* **1995**, *28*, 659.

(43) Bartolomé, J.; Filoti, G.; Kuncser, V.; Schinteie, G.; Mereacre, V.; Anson, C. E.; Powell, A. K.; Prodius, D.; Turta, C. *Phys. Rev. B* **2009**, *80*, 014430.

(44) (a) Cole, K. S.; Cole, R. H. *J. Chem. Phys.* **1941**, *9*, 341. (b) Boettcher, C. J. F. *Theory of Electric Polarization*; Elsevier: Amsterdam, The Netherlands, 1952. (c) Aubin, S. M.; Sun, Z.; Pardi, L.; Krzystek, J.; Folting, K.; Brunel, L. J.; Rheingold, A. L.; Christou, G.; Hendrickson, D. N. *Inorg. Chem.* **1999**, *38*, 5329.

(45) (a) Costes, J.-P.; Dahan, F.; Wernsdorfer, W. *Inorg. Chem.* **2006**, *45*, 5. (b) Koizumi, S.; Masayuki Nihei, M.; Shiga, T.; Nakano, M.; Nojiri, H.; Bircher, R.; Waldmann, O.; Ochsenbein, S. T.; Güdel, H. U.; Fernandez-Alonso, F.; Oshio, H. *Chem.—Eur. J.* **2007**, *13*, 8445.

(46) Pieper, H. H.; Schwochau, K. *J. Chem. Phys.* **1975**, *63*, 4716.
(47) Dobrzyńska, D.; Jerzykiewicz, L. B.; Duczmal, M.; Wojciechowska, A.; Jabłońska, K.; Palus, J.; Ożarowski, A. *Inorg. Chem.* **2006**, *45*, 10479.
(48) Krzystek, J.; Swenson, D. C.; Zvyagin, S. A.; Smirnov, D.; Ozarowski, A.; Telser, J. *J. Am. Chem. Soc.* **2010**, *132*, 5241.
(49) Mustafi, D.; Galtseva, E. V.; Krzystek, J.; Brunel, L. C.; Makinen, M. W. *J. Phys. Chem. A* **1999**, *103*, 11279.
(50) Pederson, M. R.; Khanna, S. N. *Phys. Rev. B* **1999**, *60*, 9566.
(51) Cirera, J.; Ruiz, E.; Alvarez, S.; Neese, F.; Kortus, J. *Chem.—Eur. J.* **2009**, *15*, 4078.
(52) Duboc, C.; Ganyushin, D.; Sivalingam, K.; Collomb, M.; Neese, F. *J. Phys. Chem. A* **2010**, *114*, 10750.
(53) Neese, F. *J. Chem. Phys.* **2007**, *127*, 164112.
(54) Neese, F.; Solomon, E. I. *Inorg. Chem.* **1998**, *37*, 6568.
(55) Krzystek, J.; Telser, J.; Pardi, L. A.; Goldberg, D. P.; Hoffman, B. M.; Brunel, L. C. *Inorg. Chem.* **1999**, *38*, 6121.
(56) Andres, H.; Boominar, E. L.; Smith, J. M.; Eckert, N. A.; Holland, P. L.; Munck, E. *J. Am. Chem. Soc.* **2002**, *124*, 3012.
(57) Pestovsky, O.; Stoian, S.; Bominaar, E. L.; Shan, X. P.; Munck, E.; Que, L.; Bakac, A. *Angew. Chem., Int. Ed.* **2005**, *44*, 6871.
(58) Vrajmasu, V. V.; Bominaar, E. L.; Meyer, J.; Munck, E. *Inorg. Chem.* **2002**, *41*, 6358.
(59) McGarvey, B. R. *Inorg. Chem.* **1995**, *34*, 6000.
(60) Albela, B.; Carina, R.; Policar, C.; Poussereau, S.; Cano, J.; Guilhem, J.; Tchertanov, L.; Blondin, G.; Delroisse, M.; Girerd, J. J. *Inorg. Chem.* **2005**, *44*, 6959.
(61) Chibotaru, L. F.; Hendrickx, M. F. A.; Clima, S.; Larionova, J.; Ceulemans, A. *J. Phys. Chem. A* **2005**, *109*, 7251.
(62) Chibotaru, L. F.; Ungur, L.; Aronica, C.; Etmoll, H.; Pilet, G.; Luneau, D. *J. Am. Chem. Soc.* **2008**, *130*, 12445.